Nano Scale Disruptive Silicon-Plasmonic Platform for Chip-to-Chip Interconnection

Report on characterization results of all plasmonic devices

Deliverable no.:	D6.1
Due date:	01/01/2014
Actual Submission date:	15/10/2014
Authors:	TUE/KIT/IMEC/UVEG/UGENT
Work package(s):	WP6
Distribution level:	RE[1] (NAVOLCHI Consortium)
Nature:	document, available online in the restricted area of the NAVOLCHI webpage

List of Partners concerned

Partner number	Partner name	Partner short name	Country	Date enter project	Date exit project
1	Karlsruher Institut für Technologie	KIT	Germany	M1	M36
2	INTERUNIVERSITAIR MICRO-ELECTRONICA CENTRUM VZW	IMEC	Belgium	M1	M36
3	TECHNISCHE UNIVERSITEIT EINDHOVEN	TU/e	Netherlands	M1	M36
4	RESEARCH AND EDUCATION LABORATORY IN INFORMATION TECHNOLOGIES	AIT	Greece	M1	M36
5	UNIVERSITAT DE VALENCIA	UVEG	Spain	M1	M36
6	STMICROELECTRONICS SRL	ST	Italy	M1	M36
7	UNIVERSITEIT GENT	UGent	Belgium	M1	M36

[1] **PU** = Public
PP = Restricted to other programme participants (including the Commission Services)
RE = Restricted to a group specified by the consortium (including the Commission Services)
CO = Confidential, only for members of the consortium (including the Commission Services)

Deliverable Responsible

Organization: Eindhoven University of Technology
Contact Person: Victor Dolores-Calzadilla
Address: Faculty of Electrical Engineering
P.O. Box 513
5600 MB Eindhoven
The Netherlands
Phone: +31 (0) 40247 5129
E-mail: v.calzadilla@tue.nl

Executive Summary

Several plasmonic devices were proposed within the framework of the project to be connected to each other in order to demonstrate a chip-to-chip plasmonic interconnection. Some of such devices have been successfully demonstrated whereas others remain a challenge and are still under development. This report contains the available characterization information of all plasmonic devices.

Change Records

Version	Date	Changes	Author
1 (submission)	2014-10-15		V. Calzadilla, M. Smit

1. Introduction

It is the aim of WP6 to carry out the integration, characterization and testing of the plasmonic devices intended to form the plasmonic interconnection. The devices comprise a nanolaser, a a modulator, an amplifier and a detector, from which the last three are based on plasmonic effects.

This report contains the latest characterization information of all individual plasmonic devices. When no characterization results in terms of device performance are available, characterization in terms of up-to-date fabrication results is provided. The next section provides a summary of the characterization of all devices. Section two reports the efforts to demonstrate the electrically pumped integrated nanolaser. Then, section three describes the full characterization of the plasmonic modulator, both as a phase modulator and in a Mach-Zehnder configuration. Then, the characterization results of the plasmonic amplifier and photodetector are reported in sections four and five, respectively.

2. Summary

The core technology required to fabricate the nanolaser device has been developed. Different lithography schemes were proposed and successfully demonstrated for the accurate definition of the nano-cavity, and sub-micron waveguide and grating coupler structures. Silver-based ohmic contacts were fabricated and characterized for membrane photonic circuits which showed a contact resistance as low as 0.5 10^{-8} Ωcm^2. This fabrication technology is used in the latest fabrication run that aims to demonstrate operating laser devices.

High speed plasmonic-organic hybrid (POH) Mach-Zehnder modulators are demonstrated operating at the data rates of up to 40 Gbit/s. We report on on-off keying (OOK) signaling with POH Mach-Zehnder modulators (MZM) at data rates of up to 40 Gbit/s with low energy consumptions of 75 … 225 fJ / bit. In particular, using the 29 µm device we show OOK signaling at data rates of 30 Gbit/s, 35 Gbit/s and 40 Gbit/s with the BERs well below the hard-decision FEC threshold. The measured BERs represent the lowest values, and therefore clearly demonstrating the applicability of plasmonic devices particularly in short-reach optical links. In addition, we demonstrated a latching optical switch that combines the memristor concept with plasmonics. The switch exploits the formation and elimination of a conductive path in the insulating layer of a metal – insulator – metal layer stack. The conductive path leads to an attenuation of the optical mode in the OFF state and is ruptured when switching to the ON state. The plasmonic switch is integrated with a silicon photonic waveguide. Optical extinction ratios of 12 dB at 1550 nm wavelength are shown for 10µm long devices. The operation power is consumed only when the state of the switch is changed and is below 200 nW with operating voltages in the range of 2V and currents below 100 nA. Tests with 50 write cycles and sinusoidal modulation in the megahertz regime demonstrate excellent repeatability of the switching mechanism.

Two concepts of hybrid-plasmonic amplifiers incorporating QDs (using polymer and SiN waveguides) have been fabricated and characterized by using CdSe QDs emitting at visible and HgTe QDs emitting at NIR wavelengths. Metal waveguides (planar and ridges) have been fabricated and used to investigate the observed increase of the SPP propagation length by optical pumping of QDs, even if net gain cannot be achieved by the available material.

In the case of photodetectors based on quantum dots important advances have been reached during the last year: i) reproducible and optimized conductive films of PbS QDs prepared by Dr.blading were achieved along several series of devices, ii) the best value for the responsivity in Schottky-heterostructure photodetector was around 0.16 A/W at the exciton peak absorption (≈ 1620 nm), iii) the best value of dark current was 70 nA with an ideality factor around 3, using Ag electrodes, iv) at 1550 nm, where R ≈ 0.1 A/W, pumping light above 6 nW can be detected. Plasmonic photoconductors by considering a plasmonic nano-gap waveguide concept were fabricated (in collaboration with TUe-group) and are under characterization.

3. Metallo-dielectric nanolaser

3.1. Lithography and etching processes

The definition of the nanostructure is carried out by electron-beam lithography (EBL) due to the high resolution required. This is done in three EBL steps as depicted in Fig. 1. During the first lithography, the nanopillar is defined. Later, an overlay exposure is needed to define the waveguide and, finally, the grating coupler is defined with another overlay exposure. Three different lithographic masking schemes are used during these EBL steps, which have been discussed in D1.5.

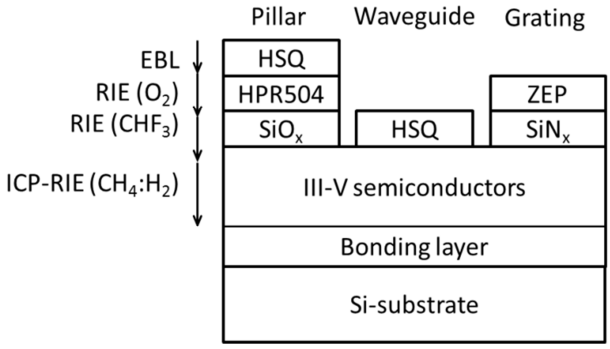

Fig. 1. Processing schemes to fabricate the different nanostructures of the laser device.

Using the semiconductor technology developed at TUe and summarized in Fig. 1, TUe has been able to fabricate the full semiconductor structure comprising the waveguide-coupled pillar cavity proposed in D3.1. The target laser structure is shown in Fig. 2b, whereas a scanning-electron microscope (SEM) picture of the latest outstanding fabrication results is presented in Fig. 2a for comparison.

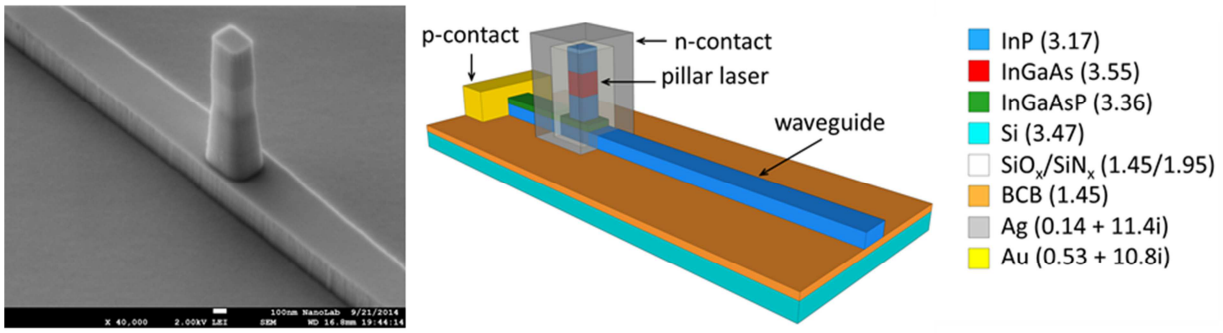

Fig. 2. SEM image of the current devices under fabrication. Right: Schematic of the target waveguide-coupled nanolaser.

Results depicted in Fig. 2 correspond to a fabrication run under progress in which only the electrical contacts are missing to complete the fabrication. The same metals deposited to fabricate the n-contact will also form the metallic cavity. This run is expected to be completed in November and fully characterized before the end of the year.

3.2. Ohmic contacts

The NAVOLCHI project targets to demonstrate sub-micron size devices. Such small devices allow, in principle, for ultra-low capacitance and therefore ultra-high speed devices as it has already been demonstrated in the plasmonic modulator reported in M14. Nevertheless, as the device size gets smaller, the contact resistance increases drastically, which puts a limitation on the voltage operation point. Therefore progress in electrical contacts is also required to develop fast nanophotonic devices compatible with standard driving electronics.

Due to the importance of the ohmic contacts in active devices, TUe has put efforts into developing suitable ohmic contacts that are compatible with plasmonic devices and provide low electrical and optical loss at the same time. For this, we studied and demonstrated low contact resistance Ge/Ag contacts. Fig. 3(left) provides a schematic of the proposed electrical contacts. Since silver itself does not adhere to InP or InGaAs, a thin layer of Germanium is required, which can be as thin as 2 nm according to our experiments. As Germanium has a high refractive index (n=4.27 at 1.5 µm), the use of a thin layer is required to minimize the modal loss due to the strong confinement.

After Ge deposition, silver is deposited by e-beam evaporation and annealed. The annealing step is done to (1) promote silver grain growth to reduce optical loss, and (2) diffuse Ge into the semiconductor layer providing additional doping to decrease the contact resistance. Special care must be taken during this annealing to avoid a deep diffusion which can cause a short circuit in p-i-n structures. Finally, a layer of gold can be sputtered to prevent silver oxidation. The full process can be done using either two lift-off processes, or one lift-off and a metal wet etching.

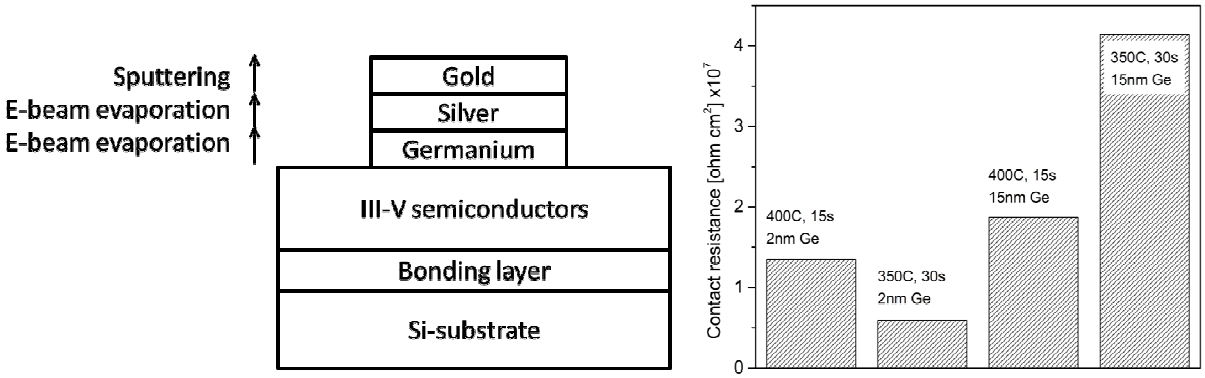

Fig. 3. Left: Schematic of Ge/Ag/Au contacts. Right: Characterization of ohmic contacts by the Transmission Line Model on n-InGaAs with doping level of $1x10^{19}$.

Experiments with the proposed silver-based contacts were done on n-doped InGaAs, which is the top semiconductor layer of the nano-cavity. The Ge layer was kept as thin as possible (2nm and 15nm), whereas the Rapid Thermal Annealing (RTA) was carried out at 350 °C and 400 °C, with 30 and 15 seconds, respectively. These annealing conditions were previously found to result in silver grain growth in III-V membranes bonded to silicon.

As it can be seen in Fig. 3(right), the lowest contact resistance is obtained when using 2 nm Ge and annealing at 350 °C for 30 seconds. In view of the high performance in terms of the contact resistance and the well-known low optical loss of silver, such contacts have been chosen to be implemented in the nanolaser device.

4. Plasmonic modulator

4.1. Plasmonic absorption modulator Conclusions

The plasmonic absorption modulator as described in deliverable 3.4 was characterized in two steps. First, we studied the quasi-static behavior. We measured the current and the optical transmission while slowly sweeping the applied voltage. In a second step, a MHz modulation was applied to the device. In summary, the device shows optical extinction ratios of 12 dB at 1550 nm wavelength for 10 µm long devices. The operation power is below 200 nW with operating voltages in the range of ±2 V and currents below 100 nA. Tests with 50 write cycles and sinusoidal modulation in the MHz regime demonstrate excellent repeatability of the switching mechanism.

4.1.1. Static behavior

We measured the current and the optical transmission as a function of the applied voltage. The voltage was applied between top and bottom electrode. A compliance current of 100 nA was set to protect the device from permanent breakdown. Continuous wave laser light at a wavelength of 1550 nm was coupled to the chip through grating couplers. The transmitted optical signal was measured with a power meter.

The electrical behavior of a 5 µm long device with the laser being turned off is displayed in Fig. 4. The applied voltage was swept from -3 V to 3 V and back in steps of 60 mV with a duration of 2 s per step. We observed a sudden increase of the current at a threshold of ~2.9 V. Here, the current reached its compliance limit. When scanning back, the current decreased while showing a hysteresis.

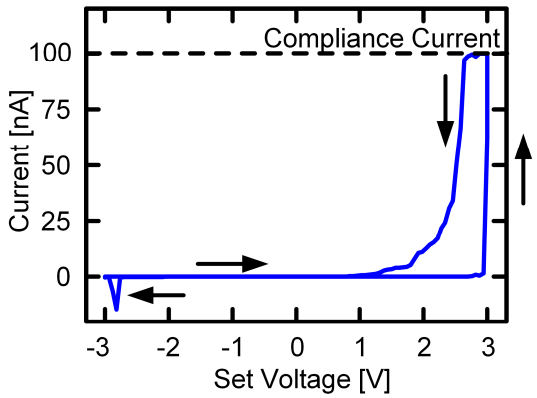

Fig. 4. Electrical current-voltage characteristic of the plasmonic absorption modulator. The response indicates a hysteresis. An abrupt increase of the current is found with a threshold around 2.9 V. Note that the set voltage differs from the actual (measured) voltage in the compliance limit.

Fig. 5(a) shows the normalized optical transmission for 50 consecutive measurement cycles below threshold (±2 V, 20 mV per step, 2 s per step, total duration of 13.3 min per cycle). We started at -2 V in the ON state. While gradually increasing the voltage, the optical signal decreased. When decreasing the voltage, the optical transmission increased again, while being lower than for the forward sweep direction. This hysteresis indicates a memory effect of the switch. The device returned to its initial state after completion of each measurement cycle. This shows excellent repeatability of the switching effect. The difference between the ON and the OFF state (extinction ratio) was 6 dB. The latching extinction ratio between the latched states was 3.5 dB. Since the device was operated below threshold, no significant current was measured and no hysteresis was observed in the I-V curve. Therefore, peak operating power during switching is below 200 nW.

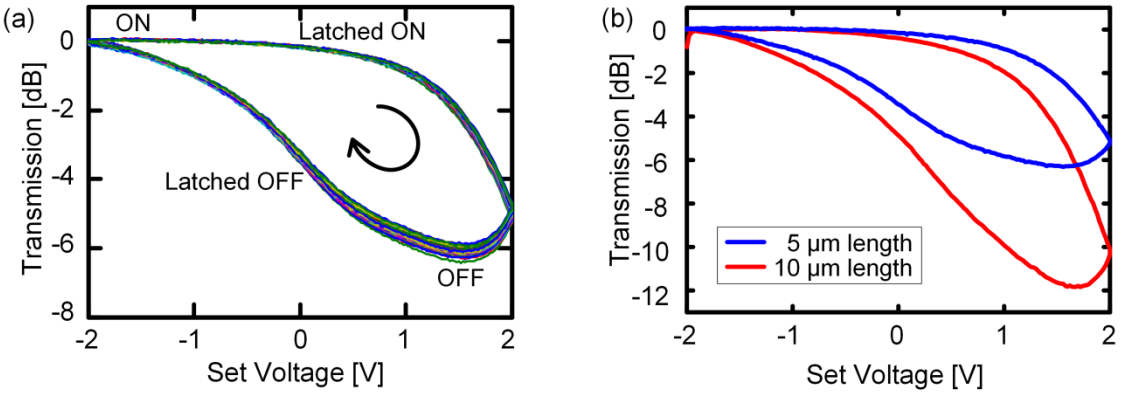

Fig. 5. Quasi-static performance of the plasmonic absorption modulator. (a) Latching optical switch behavior for a 5 µm long device: 50 measurement cycles of the normalized optical transmission as a function of the set voltage showing a hysteresis and an extinction ratio of 6 dB. (b) Latching optical switch behavior of a 10 µm long device showing an extinction ratio of 12 dB. During these measurements below threshold, no hysteresis was observed in the I-V curve.

The dependence of the extinction ratio on the device length was investigated as well. From Fig. 5(b) one can see that increasing the length from 5 µm to 10 µm increases the extinction ratio from 6 dB to 12 dB. Thus, the extinction ratio increases with increasing device length. While two devices with different lengths do not yet provide sufficient statistics the result at least indicates a trend.
Propagation losses in the hybrid waveguide section of 1 dB/µm and coupling losses between the silicon photonic and the hybrid waveguide of 6.5 dB per interface were determined through cut-back measurements.

4.1.2. Dynamic behavior

To further assess the device, we studied the dynamic behavior of the switch. Here, a sinusoidal modulation in the MHz regime was applied to the device and detected with a photodiode and a lock-in amplifier. This revealed a relatively flat frequency response between 40 kHz and 10 MHz. The 3 dB bandwidth at an operation with ± 2 V with respect the amplitude at 40 kHz is 30 MHz (see Fig. 6, blue triangles).

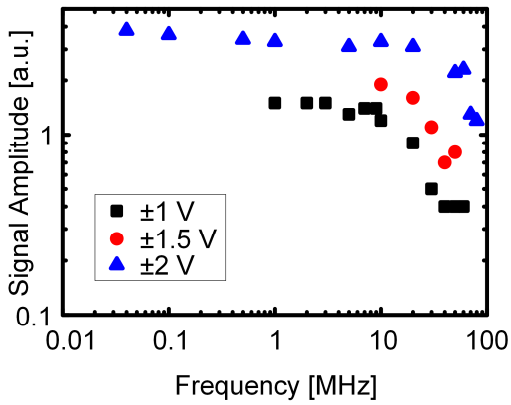

Fig. 6. MHz frequency response of the plasmonic absorption modulator. A sinusoidal signal was applied to a 5 µm long device using an arbitrary waveform generator. The optical signal was detected with a photodiode and a lock-in amplifier.

4.2. Plasmonic Mach-Zehnder modulators

The plasmonic Mach-Zehnder modulator consists of two high speed plasmonic phase shifters (see Fig. 8(a), Deliverable 3.2 and Deliverable 3.4) placed in the arms of a Mach-Zehnder interferometer realized on a silicon-on-insulator (SOI) wafer. The interferometer is designed with un-balanced arms and the operation point of the modulator is defined by the operating wavelength, see Fig. 8(b). Standard photonic multimode interference (MMI) couplers have been used as 3dB optical splitters/combiners. High speed phase modulation is performed by plasmonic phase shifters based on the Pockels effect in an electro-optic (EO) organic material, see Fig. 8(a). Applying a voltage between the metal electrodes can change the refractive index of the EO-material due to the Pockels effect, and therefore the phase velocity of the plasmonic mode. The photonic-to-plasmonic mode conversion within the arms of the Mach-Zehnder interferometer is accomplished by the metal taper couplers. Scanning electron microscope image of the active plasmonic phase shifter section is give in Fig. 8(c) and Fig. 9(a)-(c). To keep the insertion loss of

the modulators in the practical range we use low loss silicon MMI with an insertion loss of less than 0.5dB.

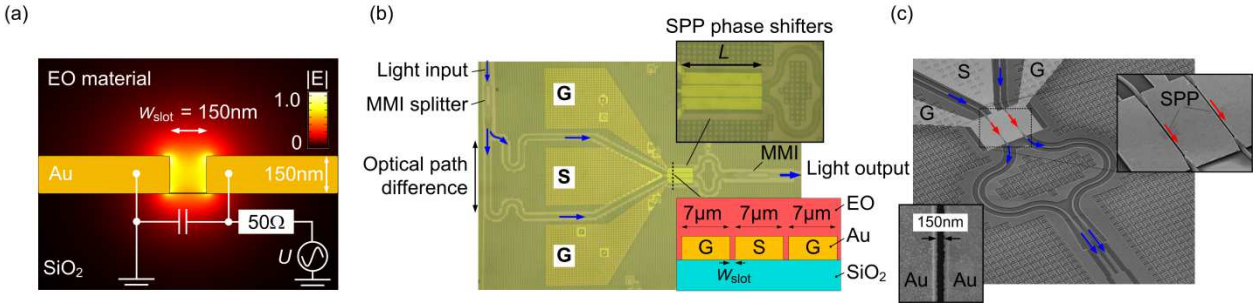

Fig. 8. Silicon-plasmonic Mach-Zehnder modulator (MZM) designed and fabricated on a silicon-on-insulator (SOI) platform. (a) Gap surface plasmon polariton (SPP) mode profile in a metal slot filled with an electro-optic (EO) material. The SPP mode is strongly confined to the slot. In addition, a lumped-element equivalent circuit of the modulator is given. Because of the high conductivity of the gold electrodes, the device can be represented by a capacitor ($C_{Device} \approx 1.5...3$ fF, L dependent). (b) Optical microscope image of the fabricated Mach-Zehnder (MZ) modulator. The MZ interferometer is defined on a passive silicon platform, where light splitting / combing is done by low loss photonic multimode interference (MMI) couplers. The photonic to plasmonic mode conversion is accomplished by metal taper couplers. An optical path difference is implemented in the MZ interferometer design to avoid applying high bias voltages. An optical phase difference between the two arms is modulated by the plasmonic phase shifters. (c) Scanning electron microscope (SEM) picture of the silicon-plasmonic MZM. The modes of the silicon waveguide are coupled to the plasmonic phase shifters, where the phases of the SPPs are modulated. In the end of the phase shifters the SPPs are back converted to photonic modes and then combined within the photonic MMI coupler

The Mach-Zehnder modulators are fabricated on a silicon-on-insulator (SOI) platform with a buried oxide with a thickness of 2mm, and a silicon device layer with a thickness of 220 nm. First, the passive silicon photonic circuit is fabricated at IMEC, in the frame work of ePIXfab, by using standard processes such as 193 nm DUV lithography and Si dry etching. The plasmonic high-speed phase shifters with a common signal electrode are defined on gold (Au). The metallic slots with the widths of ~150 nm slot and the length of 19 µm, 29 µm and 39 µm are defined with e-beam lithography and lift-off process. The slot is filled with an electrooptic material SEO100 (Soluxra, LLC). The electro-optic effect in the EO material is activated through a poling procedure. To avoid electrical breakthroughs, we perform the poling with electrical fields which are lower than the optimum poling field of 100 V/µm corresponding to the maximum r_{33} = 110pm/V.

4.2.1. Characterization results of the photonic-to-plasmonic mode converters

We first characterize the photonic-to-plasmonic mode converters using the fabricated test samples consisting of single metallic slot waveguides interfacing to silicon nanowires through two metallic taper mode converts, see Fig. 9(a) – (c). By varying the length L_{MSW} of the metallic slot waveguide between the pairs of taper couplers we can extract the conversion efficiency similar to the standard cut-back measurement. Three devices with metallic slot waveguide lengths of L_{MSW} of 1 mm, 29 mm, and 44 mm, see Fig. 9(a) – (c). The slot width is about 140 nm for all three cases.

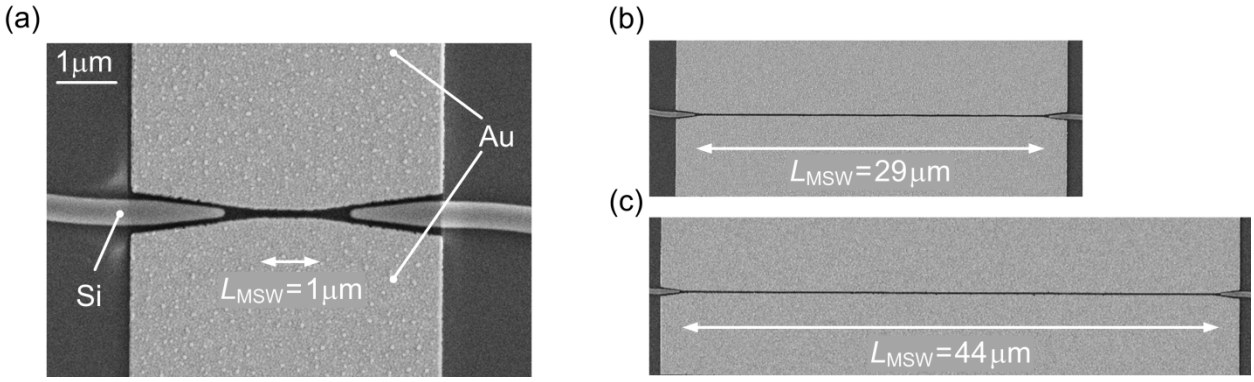

Fig. 9. Fabricated metallic tapered mode converters with three different MSW lengths LMSW of (a) 1 mm, (b) 29 mm, and (c) 44 mm. The slot size h is about 140 nm for all three devices.

The measured silicon-to-silicon waveguide transmission spectra for the three different metallic slot waveguide lengths L_{MSW} are given in Fig. 10(a). The measured transmission spectra are normalized to the measured reference spectra for a silicon strip waveguide without a plasmonic section. As can be seen, the tapered mode converters exhibit large conversion efficiency in a wide operating wavelength range. A total conversion loss of 1 dB is estimated for two transitions. This is in agreement with the theoretically expected conversion efficiency of 2…3 dB. The difference between theoretically calculated and experimentally measured conversion efficiencies is attributed to small differences of the fabricated slot widths and variations of the sidewall roughness of the metallic slots.

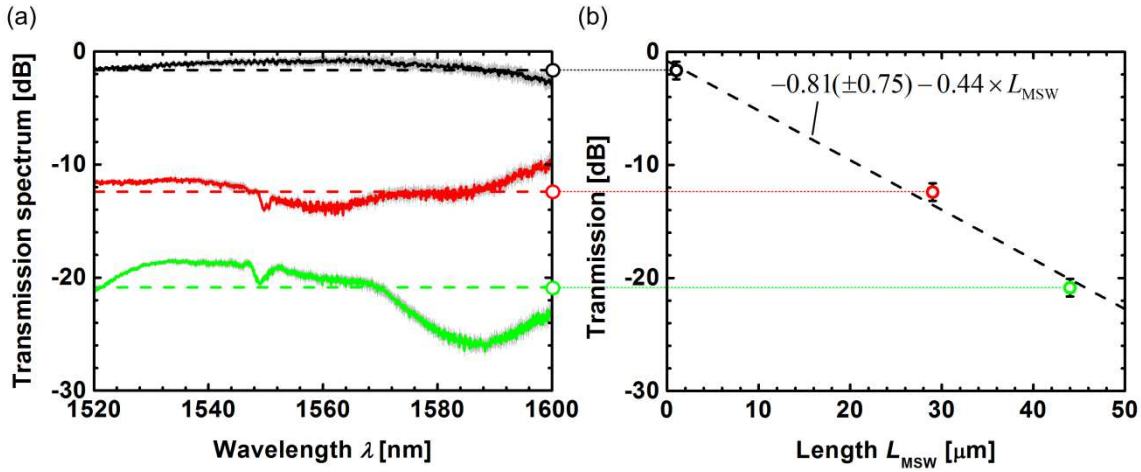

Fig. 10. Fabricated metallic tapered mode converters with three different MSW lengths LMSW of (a) 1 mm, (b) 29 mm, and (c) 44 mm. The slot size h is about 140 nm for all three devices.

4.2.2. Static behaviour of plasmonic Mach-Zehnder modulators

Power transmission spectra for all three MZMs are given in Fig. 11(a). In addition, the transmission spectrum of a reference Mach-Zehnder interferometer is given without a plasmonic phase shifter. It can be seen that, that silicon grating couplers have a big contribution in the total insertion loss of our silicon-plasmonic Mach-Zehnder modulators. With the state of the art fiber to silicon-waveguide couplers with 1dB loss the total insertion loss of the current silicon-plasmonic Mach-Zehnder modulators can be reduced down to 13-20 dB depending on the length

of the plasmonic phase shifters. The extinction ratio and the free spectral range (FSR) vary among the devices because of the uncertainty in defining the width and quality of the metallic slots. The shift of the wavelength corresponding to the minimum transmission with the applied voltage is measured in order to estimate the voltage U_p required for having a phase shift of p. An example of the transmission spectra for voltage off and on states are given in Fig. 11(b) for the MZM with the 39 µm long phase shifters. Measuring the wavelength shift Dl_0 for the applied voltage of U_0, we calculating $U_p = Dl_{FSR} \times U_0 / (2Dl_0) \approx 30$ V for MZM with 39 µm long phase shifters and that the $U_p = 37$ V for the MZM with the 29 µm long phase shifter.. In particularly, we achieve on-chip electro-optic coefficient r_{33} in the range of 70 pm/V. This value is significantly lower than the maximum value of 110 pm/V specified for bulk. These values can further be improved by optimizing the poling procedure of the EO material and improving the fabrication of the metallic slots.

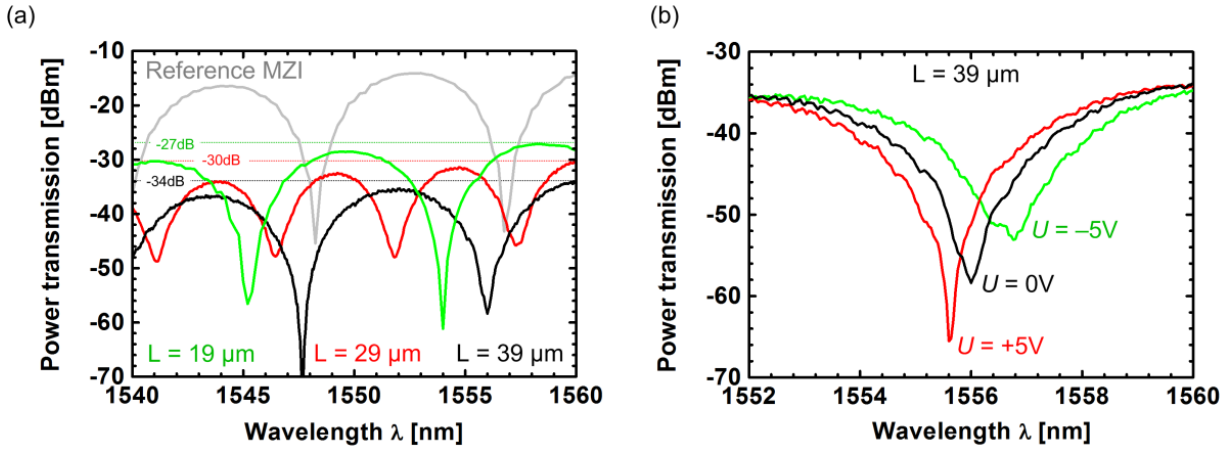

Fig. 11. Static characterization results for the Mach-Zehnder modulators. (a) Fiber-to-fiber power transmission is given for the MZMs with the length of 19 µm, 29 µm and 39 µm. In addition, we give the transmission spectrum of a reference Mach-Zehnder interferometer without a plasmonic phase shifters. The plasmonic phase shifters add 13 dB to 20 dB additional optical loss. (b) Transmission spectrum of the 39 µm long device is given for various applied voltages. Analyzing the shift of the wavelength corresponding to the minimum transmission we estimate the voltage U_p required for having a phase shift of p.

4.2.3. Data modulation

Next, data modulation experiments have been performed with the plasmonic MZM using a direct receiver setup as shown in Fig. 12(a). An electrical non-return-to-zero (NRZ) signal with PRBS pattern length of 2^{31}-1 and with a peak-to-peak voltage swing of 5 V (measured across a 50 W resistor) is fed to the modulator via a ground-signal-ground (GSG) RF probe. The operating point for the MZM is defined by selecting the operating wavelength. The MZMs are operated in the quadrature points, i.e., the modulator output intensity changes linearly with the relative phase difference of the two arms. The OOK signal after the MZM is detected with a standard pre-amplified direct receiver comprising a single erbium doped fiber amplifier, an optical band-pass filter with a bandwidth of 2 nm, a bit-error-ratio tester (BERT), and a digital communication analyzer (DCA).

We measured the BERs for all three MZMs at a bit rate of 30 Gbit/s in order to find the optimum length for the phase modulators. During the experiment, the EDFA of the receiver is operated in constant output power mode. The input optical power to the modulator is varied from +10 dBm to +23 dBm. This varies the input power to the receiver, i.e., the optical signal-to-noise power

ratio (OSNR) at the photodiodes. The optimum length of the PS is defined by a compromise between insertion loss and modulation index — making the device too short results in small optical modulation amplitude, while a too long phase modulator section decreases the receiver's input power. We find that in our case (U_{pp} = 5 V, SPP propagation losses of ~0.4 dB / µm, r_{33} = 70 pm/V) the optimum performance can be achieved with 29 µm long phase modulators, see Fig. 12(b). A better BER can be achieved by either increasing the optimum PM length L by improving the slot quality (decreasing optical losses), or by reducing the effective PM length by increasing the electro-optical coefficient and reducing the slot (increasing the optical modulation amplitude). The eye diagrams measured after the MZM with 29 µm long PM sections for bit rates of 30 Gbit/s (BER = 2×10^{-5}), 35 Gbit/s (BER = 3×10^{-5}) and 40 Gbit/s (BER = 6×10^{-4}) are given in Fig. 12(c). These BER are well below the threshold of 4.5×10^{-3} for hard-decision FEC codes with 7% overhead. The driving voltages and the optical insertion losses can be further reduced by, first, optimizing the poling procedure and thereby achieving higher electro-optic coefficients, second, reducing the slot size, and third, by using silver instead of gold.

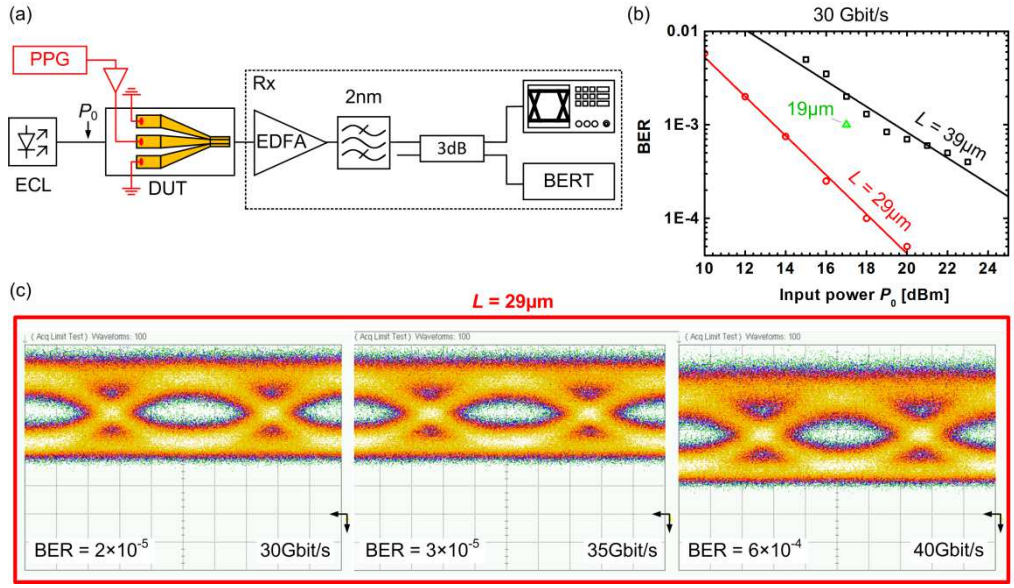

Fig. 12. Modulation experiments with plasmonic silicon-organic MZMs with PM lengths of 19 µm, 29 µm and 39 µm. (a) Direct receiver setup used for detecting on-off keyed signal after the plasmonic MZMs. (b) Bit error ratios measured for the MZMs with plasmonic phase modulator sections having lengths of 19 µm, 29 µm and 39 µm. To find the optimum phase shifter length, we vary the input power to the modulators and measure the BER. A comprise between the optical loss and the modulation index can be achieved by using a MZM with a PM length of 29 µm. (c) Eye diagrams measured at bit rates of 30 Gbit/s (BER = 2×10^{-5}), 35 Gbit/s (BER = 3×10^{-5}) and 40 Gbit/s (BER = 6×10^{-4}) for a MZM with 29 µm long PM sections at an input optical power of 20 dBm and at an operating wavelength of 1556.8 nm. The difference in the DC levels for data rates of 35 Gbit/s and 40 Gbit/s is attributed to the thermal drift of the operating point as a consequence of the large optical input power.

5. Plasmonic amplifier

5.1. Polymer based version

We have studied plasmonic structures for a direct measure of the propagation length (L_p) of the surface plasmon polariton (SPP) modes and the effect of QDs-layers on L_p, as measured by the method illustrated in Fig. 13. Figure 14 corresponds to different combinations of gold films and stripes (4 - 20 µm wide) 30 nm thick deposited on a SiO_2/Si substrate and cladded by a QD-PMMA (or bilayers QD-PMMA/PMMA) dielectric active waveguide. These waveguides allow

the study of the SPP, but not all are able to propagate the pump beam by end-fire coupling, the most optimized optical pumping of QDs inside the polymer, as previously demonstrated in our studies. This is the case of the first design (Fig. 14a), the most simple to illustrate our method to determine L_p from the signal decay of the TM mode (associated to the LR-SPP), when increasing the distance between a probe fiber tip (where a laser at 533 nm excites the photoluminescence at 600 nm of the CdSe QDs whose light couples to TM and TE modes of the waveguide) and the sample edge (Fig. 15a). The value deduced for $L_p \approx 12.5\pm2.0$ µm is very close to the theoretical one at 600 nm, $L_p \approx 11$ µm. The TE mode exhibits smaller propagation losses (associated to absorption and scattering losses in the nanocomposite) with a characteristic decay around 60 µm.

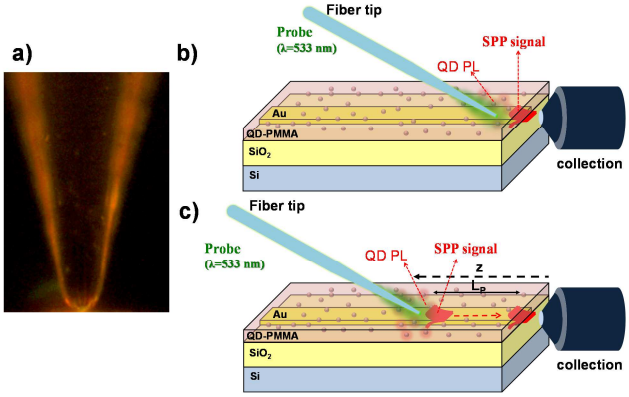

Figure 13. a) Fiber tip. b) SPP excitation with a fiber tip (533 nm at spot excites the QDs and their PL is coupled to the LR-SPP modes. c) Characterization of the Lp by measuring the intensity decay as a function of the distance between the tip and the edge of the sample.

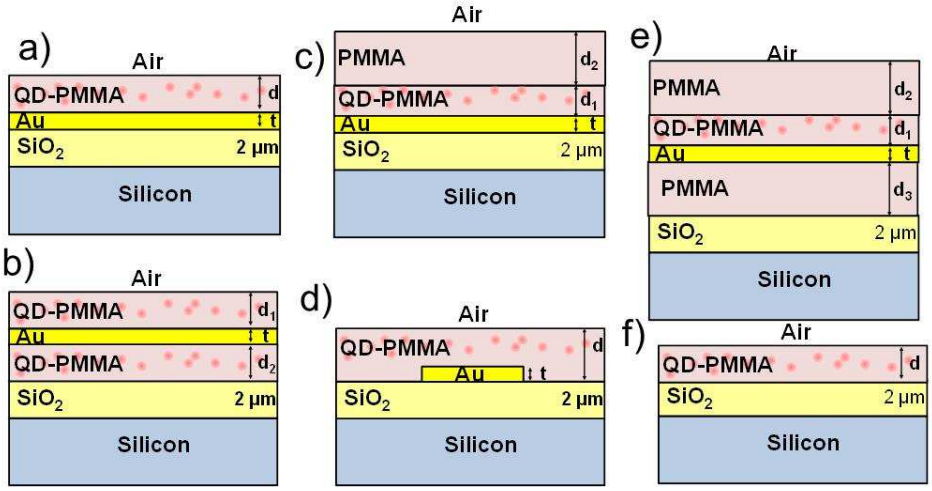

Figure 14. Vertical cross-section of different plasmonic waveguides considered in this task.

The structure depicted in Fig. 14c would allow for an efficient pumping of QD emitters along the SPP propagation; it is based on a CdSe-PMMA/PMMA bilayer cladding the Au layer. Most of the emitted light is expected to couple to the LR-SPP, because this is the mode with the highest overlap with the nanocomposite. The TM signal exhibits higher propagation losses than that of TE and hence the first is associated to the propagation of the LR-SPP. The value of Lp is estimated in the range 10.4±2.1 µm (theoretical value = 11 µm), whereas increases up to 18.4±1.7 and 25±8 µm under colinear pumping at 740 (red) and 2000 (green) W/cm^2, respectively, as deduced from results in Fig. 15b.

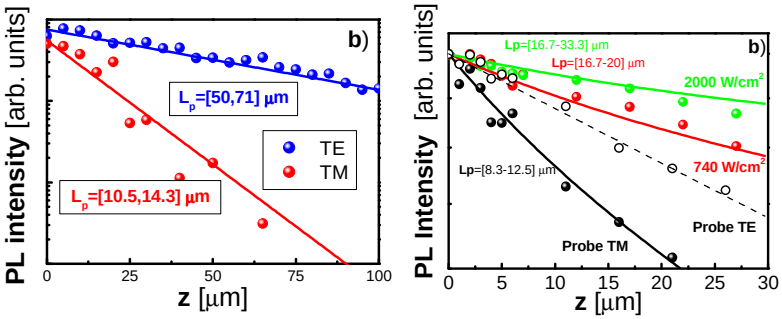

Figure 15. a) Propagation length measured at 600 nm on a Au-film waveguide 30 nm thick cladded by a QD-PMMA nanocomposite (*ff=10-3, d=1 μm*) on a SiO_2/Si substrate. b) Propagation length measured at 600 nm on a Au-film waveguide 30 nm thick cladded by a QD-PMMA/PMMA bilayer (*ff=10-3, d_1=250 nm and d_2=2.5 μm*) on a SiO_2/Si substrate without/with QD pumping at different powers.

The structure depicted in Fig. 14d was our initial focus for this project, and preliminary results were shown in the last review report (using a gold stripe several micron wide). Our results yield a value of Lp = 13±3 μm for the LR-SPP at 600 nm, which is enhanced when the pump beam is coupled in the dielectric waveguides up to 16±2 μm and 20±5 μm (for 740 and 2000 W/cm^2 of pumping power densities, respectively). More recently we have fabricated gold waveguides with some hundreds of nanometers of lateral side that will be used to finish task 4.4 by using improved HgTe QDs.

Finally, old (non-optimized) HgTe QD material was used to corroborate the enhancement of L_p in plasmonic waveguides at infrared wavelengths, even if in this range we have the limitation of a worse signal-to-noise ratio (by the use of an InGaAs photodiode array instead of a Si CCD). Plasmonic waveguides were cladded by PMMA and the HgTe-PMMA nanocomposite by using the design shown in Figure 14e (with only the bottom PMMA film to prevent metal roughness). Figure 16 shows the fiber-tip characterization in a sample with *ff* = 0.08; in tis case the symmetry of the refractive index above/below the gold layer is broken and the long range SPP is not supported. The TM signal has a clearly different intensity distribution and a larger attenuation as compared to that of TE (Fig. 16a). The dependence of the guided TM-light as a function of the distance tip-edge exhibits a double exponential decay (black data in Fig. 16b), characterized by Lp(1) ≈ 18 μm, associated to the short range SPP, and Lp(2) ≈ 67 μm that we attribute to an hybrid photonic-plasmonic mode (see D4.4). After coupling a pump beam to the input edge of the sample Lp of both modes is enhanced by a 15 % (red curve of Fig. 16b), approximately.

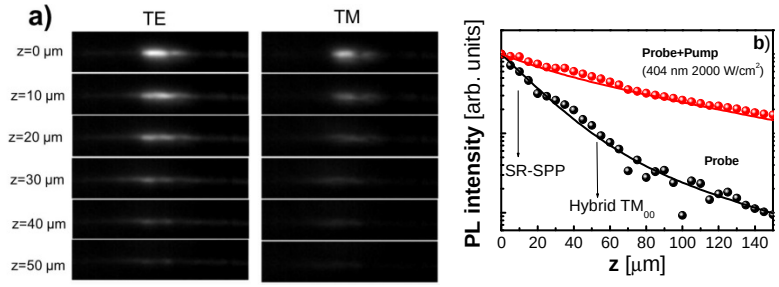

Figure 16. Near field images (a) and detected signal as a function of the fiber tip to edge distance at 1.55 μm without (black) / with (red) optical pumping of QDs (b) in the sample described in the text (*ff* = 0.08).

5.2. Hybrid silicon version

To characterize the gain of our QDs we prepared a SiN-waveguide platform allowing us to carry out a variable stripe based measurement to extract the gain. Fig. 17a shows SiN partly covered

with CdSe QDs (increasing length from top to bottom). Fig. 5b shows the measurements for one set of waveguides, under CW pumping. In case of gain this curve should show a superlinear trend, which is not the case here. We are currently preparing a setup to pump these devices under pulsed conditions with high peak power.

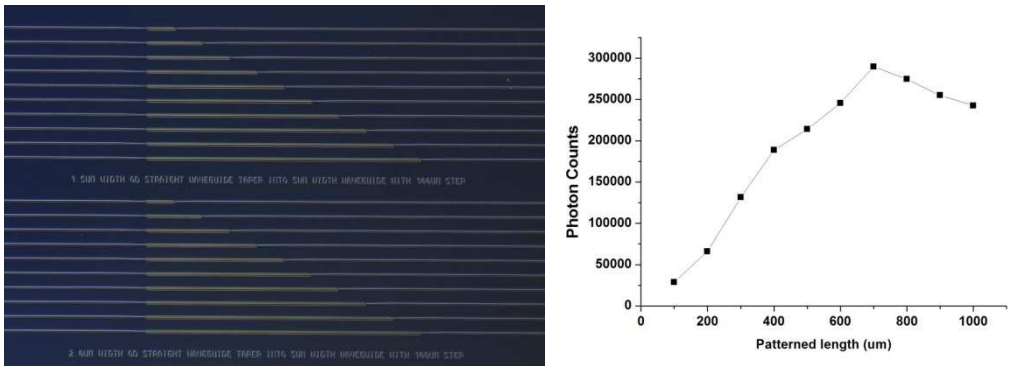

Figure 17. a) Microscope view of SiN with variable length QD-pattern on top. b) Power emitted at 600 nm as function of length.

6. Plasmonic photodetector

6.1. Schottky-heterostructure photodiodes

In the last months we have optimized the synthesis of PbS QDs with absorption/emission at wavelengths around 1550 nm, as also the deposition (+ ligand exchange) of thin films in the thickness range 300-500 nm by means of a Dr.Blading technique. These layers exhibit a reasonable uniformity throughout the sample, as revealed by exciton absorption and photoluminescence (PL) spectra very close to those in colloidal solution. Layers with completed ligand exchange have a resistivity around 10^5 □cm, a hole concentration larger than 10^{15} cm^{-3} and mobilities smaller than 0.065 cm^2/Vs, as estimated from preliminary Hall measurements.
These Schotky diodes have been characterized under laser illumination at 1550 nm as a function of power (Fig. 18). The I(V) characteristics exhibits can be fitted by using a real equivalent circuit for the photodiode that yields a dark current around 70 nA with an ideality factor around 3 (carrier generation-recombination mechanism) and shunt resistance (attributed to hole losses through the Ag electrode) decreasing with increasing illumination. The lowest detected power was 6 nW by using our Keithley 2400 source-meter, hence the noise equivalent power is smaller than this value (under continuous wave excitation). The photocurrent is practically linear (exponent = 0.92) with power from 6 nW (I_{cc} = 0.8 nA, V_{oc} = 9 mV) to 2 µW (I_{cc} = 190 nA, V_{oc} = 70 mV) and R ≈ 0.1 A/W in the entire range. The newest generation of photodiodes (under characterization) will serve us to measure other important parameters and figures of merit for Schottky-heterostructure photodiodes and characterization as a function of temperature, prior to introduce a stopping layer for holes (to increase fill factor, reduce noise current and increase of V_{oc}) and plasmonic effects (to increase light trapping and near-field absorption at the QD layer.

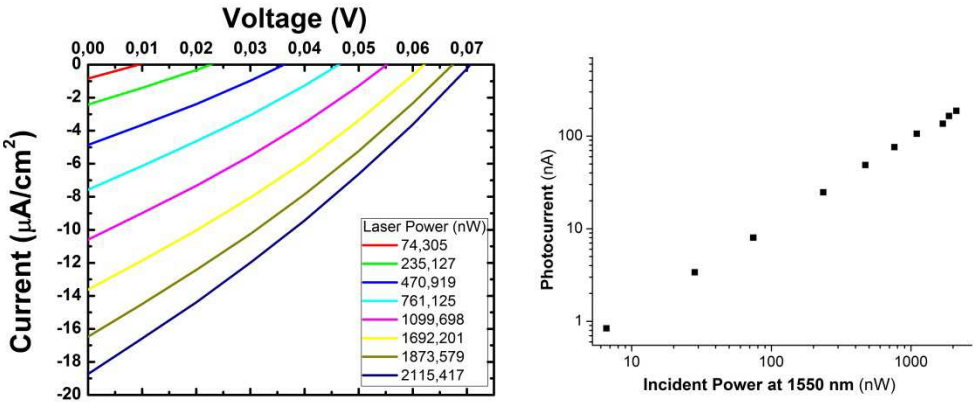

Figure 18. (a) I(V) characteristics of the best ITO/PDOT/PbS-QD-solid/Ag photodiode (at 1550 nm) under illumination with a laser at 1550 nm at different powers; (b) power dependence of the measured photocurrent.

6.2. QD-solid based microgap/nanogap photoconductors

The Schottky concept is a very convenient device to be integrated in SOI technology, because photocurrent or photovoltage can be directly measured without needing of polarization or used as input for a transimpedance amplifier. Given that most of the work on Schottky diodes is already finished our goal is to concentrate our effort on photoconductive devices. In the case of nanogap, given the small distance between electrodes and high electric field we do not plan to use ligand exchange on deposited QDs. In the case of microgap we have develop a first generation of interdigitated electrodes, for which appreciable photocurrent is measured at 1550 nm in preliminary tests, even if we are not satisfied with the ligand exchange protocol on small area QD-layers. In this sense, in a photoconductive device (0.2 mm gap) made these days on a QD-layer prepared as in the Schottky device (complete ligand exchange) we arrive to photocurrents ≈ 30-50 nA (responsivities very close to 0.1 A/W) in the wavelength range 1200-1500 nm at 200 V bias, despite the big distance between electrodes, over a reasonably low dark current (49 nA).

Next steps are the improvement of microgap photoconductor devices by means of developing a good protocol for ligand exchange in the QD-film and concentrate on plasmonic nanogap-waveguide photoconductors for which a first fabricated series is under investigation. Given the background layer of ITO deposited on a glass substrate and the small distance between electrodes (50-70 nm) bias voltage is limited between -0.5 to + 0.5 V.